

## Unzipping bird feathers

Alexander Kovalev, Alexander E. Filippov and Stanislav N. Gorb

*J. R. Soc. Interface* 2014 **11**, 20130988, published 18 December 2013

---

### Supplementary data

["Data Supplement"](#)

<http://rsif.royalsocietypublishing.org/content/suppl/2013/12/17/rsif.2013.0988.DC1.html>

### References

[This article cites 17 articles, 1 of which can be accessed free](#)

<http://rsif.royalsocietypublishing.org/content/11/92/20130988.full.html#ref-list-1>

### Email alerting service

Receive free email alerts when new articles cite this article - sign up in the box at the top right-hand corner of the article or click [here](#)

## Research



**Cite this article:** Kovalev A, Filippov AE, Gorb SN. 2014 Unzipping bird feathers. *J. R. Soc. Interface* **11**: 20130988.  
<http://dx.doi.org/10.1098/rsif.2013.0988>

Received: 26 October 2013

Accepted: 26 November 2013

### Subject Areas:

biomechanics, computational biology, biomaterials

### Keywords:

feather, interlocking, numerical model

### Author for correspondence:

Alexander Kovalev

e-mail: [akovalev@zoologie.uni-kiel.de](mailto:akovalev@zoologie.uni-kiel.de)

Electronic supplementary material is available at <http://dx.doi.org/10.1098/rsif.2013.0988> or via <http://rsif.royalsocietypublishing.org>.

# Unzipping bird feathers

Alexander Kovalev<sup>1</sup>, Alexander E. Filippov<sup>2</sup> and Stanislav N. Gorb<sup>1</sup>

<sup>1</sup>Functional Morphology and Biomechanics, Department of Zoology, Kiel University, Kiel 24118, Germany

<sup>2</sup>Department of Electronic and Kinetic Properties of Non-linear Systems, Donetsk Institute for Physics and Engineering, National Academy of Science, Donetsk 83114, Ukraine

The bird feather vane can be separated into two parts by pulling the barbs apart. The original state can be re-established easily by lightly stroking through the feather. Hooklets responsible for holding vane barbs together are not damaged by multiple zipping and unzipping cycles. Because numerous microhooks keep the integrity of the feather, their properties are of great interest for understanding mechanics of the entire feather structure. This study was undertaken to estimate the separation force of single hooklets and their arrays using force measurement of an unzipping feather vane. The hooklets usually separate in some number synchronously (20 on average) with the highest observed separation force of 1.74 mN (average force 0.27 mN), whereas the single hooklet separation force was 14  $\mu$ N. A simple numerical model was suggested for a better understanding of zipping and unzipping behaviour in feathers. The model demonstrates features similar to those observed in experiments.

## 1. Introduction

The feather of modern birds is an epidermal outgrowth having complex structure, which evolved since the Late Jurassic [1]. The feather was inherited by birds from a common ancestor of birds and crocodylians, because it demonstrates the presence of a homologous trait in both animals groups [2]. The theropod dinosaurs, closest related to birds, have pinnate feathers, while the feathers of theropods that are distantly related to birds are simple filaments or bunches of filaments of varying lengths and diameters. These hollow filaments or protofeathers are similar to structures seen in feather development: a hollow cylindrical sheath arises first in feather ontogeny from the collar of the feather follicle before the barb ridges [1].

The main function of feathers in birds and their ancestors is to support flight. However, discovery of non-flying Late Cretaceous feathered dinosaurs suggests that display function played a key role in the early evolution of pinnate feathers [3]. The coloration of feathers is believed to have primarily evolved in response to sexual selection, as it is shown for modern birds [4]. Thermoregulation or waterproofing could have been the original primary functions at least in smaller dinosaurs [5,6]. This is supported by the fact that feather density in smaller birds is higher than in larger birds, because smaller birds lose more heat owing to the relatively larger surface area in proportion to their body volume [7].

The feathers of modern birds are a waterproof, breathable, lightweight construction combining thermal isolation, rigidity and flexibility [8,9]. These properties are partly related to the feather's ability to hold its parts together temporarily by an elaborate pattern of microhooks (hooklets). Such feather interlocking devices are well known from zoology textbooks [10]. The feather vane (plane part) can be separated into two parts by pulling neighbouring barbs apart. The original state can be re-established easily by lightly stroking through the feather.

The vane of a typical contour feather consists of a number of side branches called barbs, aligned parallel to each other and at an angle to the shaft. The barbs carry, on either side, a similar array of second-level side branches called barbules. In most birds, the row of barbules on the side of the barb towards the tip of the feather bears very fine, backward facing hooklets, as one can see on scanning electron microscopy (SEM) images (figure 1*a,b*). These barbules are called hook barbules. The barbules on the other side of the barb are sharply curved and have

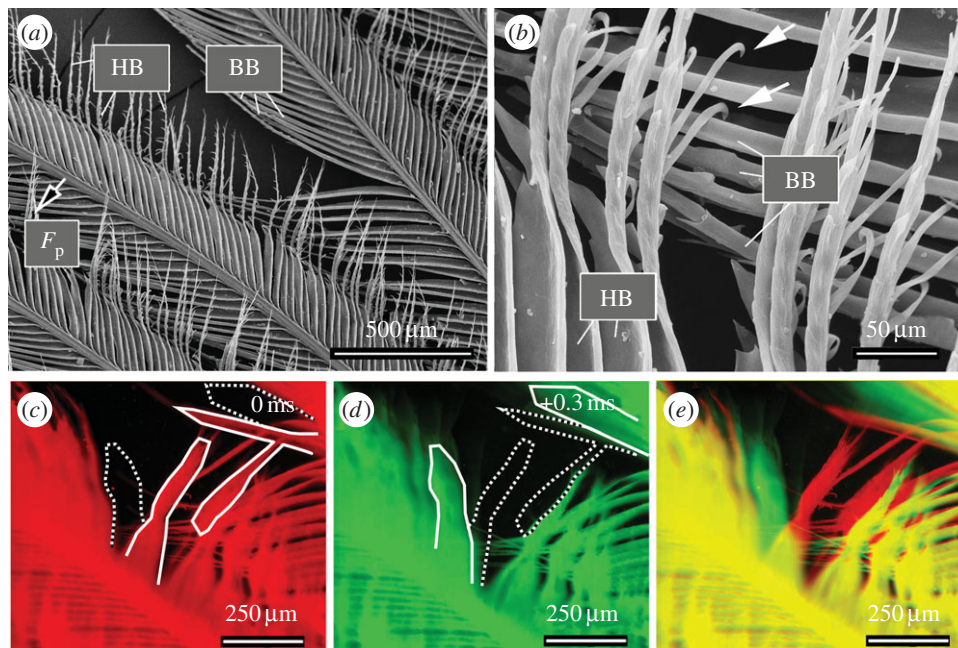


**Figure 1.** (*a, b*) Structure and (*c–e*) rupture of a feather. (*a, b*) Scanning electron micrographs showing the anchoring between hook barbules, HB, and bow barbules, BB. The pulling force,  $F_p$ , indicated by a black arrow is applied to a lower barb whereas the upper barb is fixed. (*c–e*) Optical microscopy based single frames of a high speed videorecording of the feather crack area before (*c*) and 0.3 ms after (*d*) rupture event (see also electronic supplementary material, movie S1). The white contour in (*c*) marks initial positions of moving barbules. The new positions of barbules are shown by dotted lines. The white contour in (*d*) marks the final positions of moving barbules, whereas dotted lines show their initial positions. The shutter time is 0.1 ms. (*e*) The superposition of images (*c*) and (*d*). Yellow colour is for immobile feather elements. Red is for the initial and green for the final positions of moving feather elements.

only very short spine-like outgrowths (bow barbules). Hook barbules become automatically anchored on the bow barbules, owing to the preferred orientation of the hooklets and micro-irregularities on both types of barbules.

The separation of the barbules can be caused by some external force. This protects the feathers from real damage and provides the easy repair of a microrupture in the feather coverage. Although the structure and function of the system are well known in general, the rupture forces have not been rigorously measured. Because numerous feather microhooks keep the integrity of the feather, their collective properties are of great interest for understanding rupture/recovery mechanics of the entire feather. Behaviour similar to the collective behaviour of microhooks at feather rupture is observed in many different processes, such as, for example, in the motion of the main plasticity carriers [11] or in Barkhausen noise in ferromagnetic materials [12].

This study was performed in order to obtain information about the rupture force dynamics affected by the cooperative hook's behaviour from force measurements and from a numerical model of an unzipping feather vane.

## 2. Material and methods

Pennaceous feathers of the swan (*Cygnus olor*) were used for the force measurements (figure 2). The feather was clamped at its vane in a position such that barbs were oriented parallel to the ground. The tip of the next free barbule was clamped to the force sensor (load cell force transducer, FORT 10, World Precision Instruments, Sarasota, FL, USA). The force sensor was attached to a motorized micromanipulator (DC3001R, World Precision Instruments) similar to [13]. Vertical displacement of the transducer using a micromanipulator caused separation of two

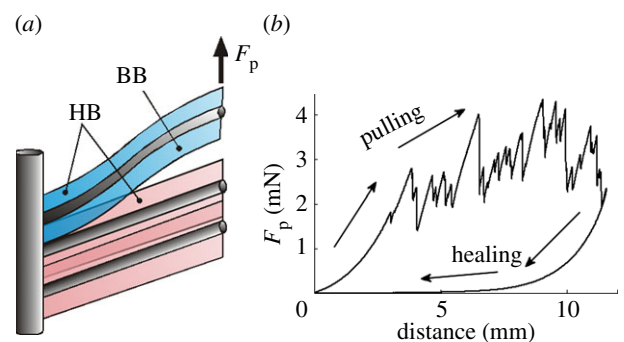


**Figure 2.** (*a*) Scheme of the experimental set-up and (*b*) the force–distance diagram of the force measurement. The feather was separated (pulling) at the interface between two neighbouring barbs using a micromanipulator equipped with a load cell force transducer attached to the margin of the vane. This separation caused detachment of hook barbules (HBs) from bow barbules (BBs). Arrow indicates direction of the pulling. After some final displacement was reached the force transducer was moved back (healing). (Online version in colour.)

neighbouring barbs, figure 2*b*, pulling. Separation was performed with a speed of  $200 \mu\text{m s}^{-1}$ . Afterward, the force sensor was moved to its initial position, figure 2*b*, healing. Ten such measurements were performed on five individual feathers at the force sampling frequency of 1 kHz. The video of the barbule separation process in pennaceous feathers of swans and a rectrice of a pigeon (*Columba palumbus*) was recorded with 10 000 frames per second ( $50 \mu\text{s}$  exposition) using a high-speed camera (Photron Fastcam SA1) mounted on an inverted microscope Axio Observer.A1 (Carl Zeiss MicroImaging GmbH, Jena, Germany).

Feather material was collected from different sources (a laboratory collection) and stored in sealed plastic bags at room temperature prior to use. The numerical simulations were performed using Matlab v. 7.10 (The MathWorks, Natick, MA, USA).

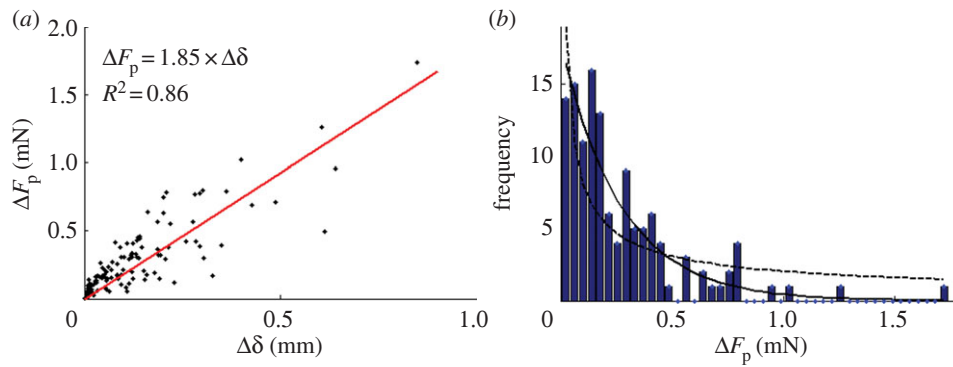


**Figure 3.** (a) Dependence of the force required for a single separation event ( $\Delta F_p$ ) on the pulling distance ( $\Delta\delta$ ) travelled by the force sensor. (b) Frequency histogram of  $\Delta F_p$ . One hundred and twenty-six force peaks were measured on five feathers. Histogram was fitted with an exponential function,  $17.9e^{-3.56\Delta F_p}$  ( $\chi^2 = 105$ ; solid line), and with a power function,  $2.05\Delta F_p^{-0.6}$  ( $\chi^2 = 326$ ; dashed line). (Online version in colour.)

### 3. Results

#### 3.1. Experimental results

High-speed video recording of the feather rupture process demonstrated that because barbules are oriented at some angle to barbs, the barbules were bent near their bases during feather stretching; compare left upper (free) and right lower (fastened) corners (figure 1c). Normally, during the feather stretching, the bending of the linked barbules increases, and at a certain point, the linked barbules uncouple from one another (figure 1c–e). The uncoupling process is very quick and takes just less than 0.1–0.3 ms. Previously deformed barbules return to their initial positions. During the feather stretching (rupture), figure 2a, the individual barbule separation events are seen as force drops, figure 2b. When the pulling force decreases to zero, the barbs return to their initial positions guided by the elastic forces, figure 2b, and anchoring between hooks and bow barbules recovers (healing process). The hysteresis of a force–distance curve at pulling/healing, figure 2b, occurs because barbule bending takes place at pulling but not at healing.

Force and stretching distance increments between uncoupling events (force drops) could be determined from the force–distance curves (figure 2b). The force-to-separation distance ratio remains constant ( $1.85 \text{ N m}^{-1}$ ; figure 3a). This means that typically many barbules are involved in the separation process. The distribution of the hooklet connection strength should also be important. Because root mean square of the noise level was  $1.5 \mu\text{N}$ , we were able to detect events of the separation of single hooklets. The distribution of force increments shows that events of single hooklet separation approximately correspond to a force of about  $14 \mu\text{N}$  (see electronic supplementary material, figure S2). The force measurements demonstrate that a few hooklet separation events are most frequently observed (figure 3b). In the experiment, not single hooklets, but their clusters mainly separated from the counterpart barb at once. Average force increment, resulting from the separation of multiple hooklets, was  $0.27 \text{ mN}$  (s.d. =  $0.27$ ,  $n = 126$ ). The highest force increment was  $1.74 \text{ mN}$ . Assuming that the force increments are proportional to the number of hooklets holding barbs together before the next uncoupling event takes place, the number of simultaneously separating hooklets can be estimated from the measured pulling force and from the force necessary for single hooklet separation. So, while pulling the row of barbules, 1–40 hooklets (mean =  $19.4$ , s.d. =  $19.4$ ,  $n = 126$ ) were separated at once.

On average, 0.79 hooklets (s.d. =  $0.73$ ,  $n = 158$ , up to 3.5 hooklets) were separated at once at a pulling distance of  $100 \mu\text{m}$ . The histogram of force increments was fitted with a power law and an exponential function. The exponential fit has lower value of  $\chi^2$  (figure 3b).

Further, a dynamical mathematical model is introduced, which qualitatively describes zipping/unzipping behaviour in a feather. Using this model, the dynamics of the number of hooklets uncoupling during a feather stretching and statistical properties of the rupture forces were analysed.

#### 3.2. Mathematical model

Our discrete numerical model describes the dynamics of two initially parallel aligned elastic barbs. The conceptual structure of the model is shown in figure 4, and the model parameters and their description are summarized in table 1. Each barb was constructed of 100 elastic segments, each having a length of  $dR = 60 \mu\text{m}$ , figure 4b, according to the measurements on SEM images (figure 1a,b). The barbs were provided with longitudinal ( $K^{\parallel}$ ) and transverse ( $K^{\perp}$ ) stiffness,  $K^{\parallel} = K^{\perp}$ . Transverse stiffness tends to hold the angle between the neighbouring segments close to  $180^\circ$ .

As in a real feather, the barbs in the model carry barbules. We constructed the barbules in a manner similar to that in the real barbs. Each of the barbules is elastically attached to a barb. In the model, each barbule was constructed of 10 segments. According to the measurements on SEM images the segment's length ( $dr$ ) was taken the same as for the barbs,  $dr = dR$ . In feathers, the barbules are oriented at some angle to the barbs. The barbules in the model were oriented at  $\beta_{01} = 30^\circ$  (bow barbules, upper side) and  $\beta_{02} = 45^\circ$  (hook barbules, lower side), figure 4b. The barbules and barbs have different thickness and therefore different values of their elastic constants,  $K^{\parallel}$  and  $K^{\perp}$ . Based on the SEM images, we assume that the barbules have approximately 10 times lower transverse and the same longitudinal elastic constants compared with the barbs:  $k^{\parallel} = K^{\parallel}$ ,  $k^{\perp} = 0.1K^{\perp}$ . Such approximation allows emphasizing the bending degree of freedom and retaining other geometrical parameters about constant.

As in the experiment, the top right tip of the barb, figure 4a, was moved with constant velocity,  $V = 50 \mu\text{m s}^{-1}$ , until the tip reached the final displacement of  $2.1 \text{ mm}$ . After this, the barb was released and returned spontaneously to its initial position. Low separation velocity compared with velocity of internal motions (for both real and numerical experiments) considerably reduces inertia effects.

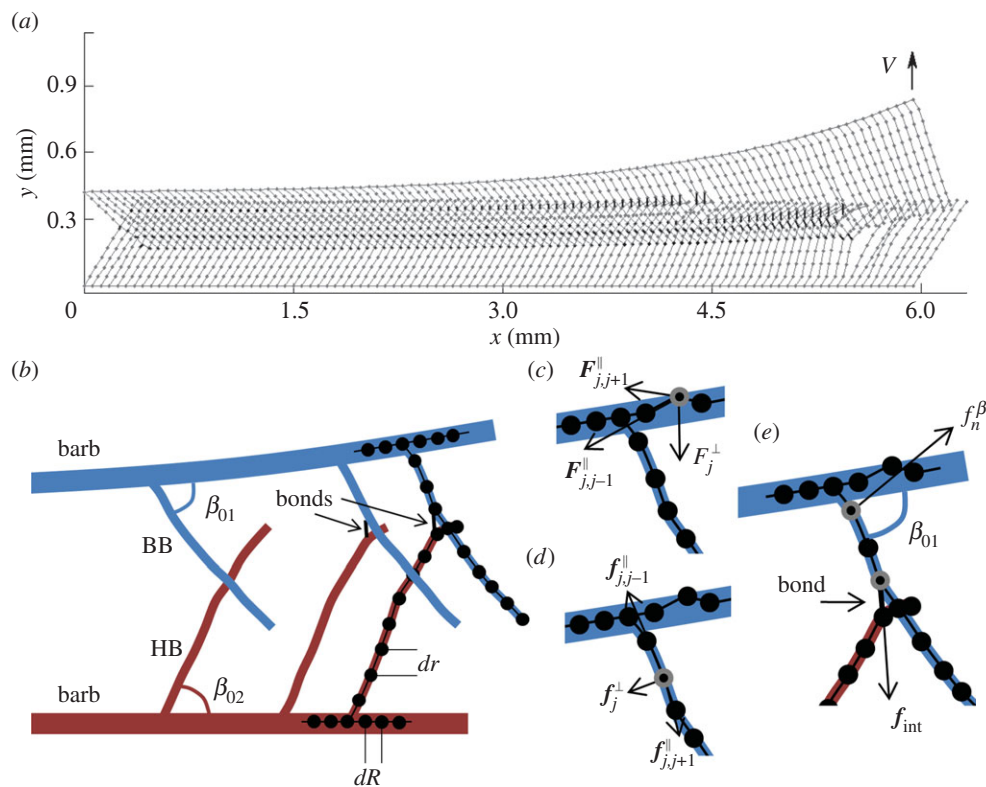


**Figure 4.** Conceptual structure of the model. (a) Two connected elastic subsystems of the fibres simulating barbs with barbules are shown by the grey lines. The nodes and elastically connected segments are respectively shown by the grey circles and grey lines. The pairs of instantly interacting nodes from two different subsystems (which are close enough to build an interaction bond by meshing the hooks) are connected by the bold black lines. The arrow shows that the right terminal point of the upper subsystem is attached to an external cantilever, which is moving with constant velocity  $V$  (see also the electronic supplementary material, movie S2). Schematic of the structural parameters (b) of the mathematical model and forces (c–e) presented in the model.  $dR$  is segment length of barbs,  $dr$  is segment length of barbules,  $\beta_{01}$  and  $\beta_{02}$  are the equilibrium angles between a barb and a hook barbule (HB) or bow barbule (BB), respectively. The forces are shown only for selected nodes (small black circle inside grey circle). (c) Longitudinal  $F_{jk}^{\parallel}$  and transverse  $F_j^{\perp}$  forces acting on a barb node  $j$ . Longitudinal force depends on interaction of node  $j$  with its neighbours  $j - 1$  and  $j + 1$ . (d) Longitudinal  $f_{jk}^{\parallel}$  and transverse  $f_j^{\perp}$  forces acting on a barbule node  $j$ . (e) Rotational force  $f_n^{\beta}$  acting on adjacent segments of a barbule and a barb, which tends to keep the joint angle constant. Interaction force  $f_{\text{int}}$  tends to keep the initial orientation of bound segments on HB and on BB.

A deformation of barbs produces elastic forces proportional to the barb stiffness, figure 4c. The forces are described by the following equations:

$$F_{jk}^{\parallel} = K^{\parallel}(\mathbf{R}_j - \mathbf{R}_k) \left[ 1 - \frac{|\mathbf{R}_j - \mathbf{R}_k|^2}{dR^2} \right]$$

$$\text{and } F_j^{\perp} = K^{\perp}(2\mathbf{R}_j - \mathbf{R}_{j+1} - \mathbf{R}_{j-1}), \quad (3.1)$$

where  $\mathbf{R}_j$  is a position vector of the middle of the segment (the node)  $j$ ;  $k = j \pm 1$ . Longitudinal force,  $F_{jk}^{\parallel}$ , according to this equation, tends to keep a distance between the nodes  $\mathbf{R}_j$  and  $\mathbf{R}_{j\pm 1}$  close to the equilibrium length of the segment  $dR$ , and it is linear at small displacements (see electronic supplementary material, figure S1). Transverse force,  $F_j^{\perp}$ , is directly proportional to the lateral deflection and tends to keep  $\mathbf{R}_j$  close to the mean value between its nearest neighbours,  $(\mathbf{R}_{j+1} + \mathbf{R}_{j-1})/2$ . The transverse force in the present form is easy to realize, but it is not a purely bending force, because it may include a longitudinal component.

The segments of barbules are connected by the forces described in the same way as the forces between segments of the barbs (equation (3.1)), figure 4c,d:

$$f_{jk}^{\parallel} = k^{\parallel}(\mathbf{r}_j - \mathbf{r}_k) \left[ 1 - \frac{|\mathbf{r}_j - \mathbf{r}_k|^2}{dr^2} \right]$$

$$\text{and } f_j^{\perp} = k^{\perp}(2\mathbf{r}_j - \mathbf{r}_{j+1} - \mathbf{r}_{j-1}), \quad (3.2)$$

where  $\mathbf{r}_j$  is a position vector of the barbule's node  $j$ ;  $k = j \pm 1$ .

Additionally, a barbule–barb joint rotational stiffness,  $B$ , was introduced, which tends to keep the joint angles,  $\beta_n$ , constant. The rotational force, figure 4e, acting on adjacent segments of the barb and barbules is linearly proportional to the difference  $\beta_{0n} - \beta_n$ :

$$f_n^{\beta} = B(\beta_{0n} - \beta_n), \quad (3.3)$$

where index  $n = 1, 2$  numerates the barbs. At  $B > 0$ , the force in equation (3.3) tends to keep the angle as close to the equilibrium value as possible. As a result, the system dynamically maintains a shape similar to the one depicted in figure 4a.

The main feature of the feather is that bow and hook barbules stay connected during pulling until some critical force/displacement is achieved in the connection between hooklets and short spines. To simulate this, in the model, we assume that if a node of a hook barbule is close enough to nodes of the bow barbules, then it can form a 'bond' (connection between hooklet and spines, figure 4a,b,e). For the sake of simplicity, in an initial state, all possible bonds appear at a certain distance between the barbule segments.

The bonds can be characterized by the vectors  $\mathbf{r}_{nm} = \mathbf{r}_n - \mathbf{r}_m$ , where indices  $n$  and  $m$  numerate the contacting nodes on both subsystems (hooklets and spines on bow barbules) and  $\mathbf{r}_n$  and  $\mathbf{r}_m$  are position vectors of the nodes. When one end of a barb starts to move vertically, it pulls barbule segments from their initial position to a new one. This deformation causes an interaction force  $f_{\text{int}}$ , figure 4e, which tends to return the

**Table 1.** Parameters of the mathematical model of the feather and their descriptions.

parameter	description
$\mathbf{R}_j, \mathbf{r}_j$	position vectors of barb and barbule nodes
$dR, dr$	equilibrium segment length of barbs and barbules
$K^{\parallel}, k^{\parallel}$	longitudinal stiffness of barb and barbule segments
$\mathbf{F}_{jk}^{\parallel}, \mathbf{f}_{jk}^{\parallel}$	longitudinal forces acting on barb and barbule segments
$K^{\perp}, k^{\perp}$	transverse stiffness of barb and barbule segments
$\mathbf{F}_j^{\perp}, \mathbf{f}_j^{\perp}$	transverse forces acting on barb and barbule segments
$\beta_{01}, \beta_{02}$	equilibrium angle between bow/hook barbules and barbs
$\beta_n$	actual angle between barbules and barbs
$B$	barbule–barb joint rotational stiffness
$f_n^{\beta}$	rotational force acting on adjacent segments of barbs and barbules
$\mathbf{r}_{0n}$	equilibrium position vector of barbule nodes building a bond
$\mathbf{r}_{0nm}$	an equilibrium bond vector
$\mathbf{r}_n$	actual position vector of barbule nodes building a bond
$\mathbf{r}_{nm}$	an actual bond vector
$k_{\text{int}}$	bonds' stiffness
$f_{\text{int}}$	bonds' interaction force
$r_{\text{th}}$	threshold value of a bond deformation
$\bar{r}_{\text{th}}$	maximum value of the threshold value of a bond deformation
$V$	pulling velocity of the feather tip
$\gamma$	damping coefficient
$M$	mass of segment
$F$	the total interaction force between two barbs
$N(t)$	total number of connected bonds to the time $t$
$\langle dN/dt \rangle_{\tau}$	time derivative of function $N(t)$ averaged over time interval $\tau$

distance between bound barbules to equilibrium. For small deviations,  $f_{\text{int}}$  linearly increases with the distortion:

$$\mathbf{f}_{\text{int}} = k_{\text{int}}(\mathbf{r}_{0nm} - \mathbf{r}_{nm}), \quad (3.4)$$

where  $k_{\text{int}}$  is a stiffness of the bond,  $\mathbf{r}_{0nm}$  is the equilibrium bond vector. At large deformations, the interaction force  $\mathbf{f}_{\text{int}}$  also becomes strong, and the hooklets detach. In the framework of this model, it means that if deformation exceeds some threshold value  $r_{\text{th}}$ :

$$|\mathbf{r}_{0nm} - \mathbf{r}_{nm}| \geq r_{\text{th}}, \quad (3.5)$$

then the bond breaks. In a real system, the threshold depends on the spatial realization of the particular contact and is different for different interconnections. In the model, it could be realized by a random distribution of the thresholds:

$$r_{\text{th}} = r_{\text{th}}\xi, \quad (3.6)$$

where  $r_{\text{th}}$  is a constant,  $0 < \xi < 1$  is a uniformly distributed random number. For further simulations, we take  $k^{\parallel} = 2.4k_{\text{int}}$ ;  $r_{\text{th}} = dR$ . The force-to-separation distance ratio was found to be in good agreement with experimental data for such a relation between  $k^{\parallel}$  and  $k_{\text{int}}$  (see Discussion). Figure 4a reproduces the described model system in some intermediate configuration.

A single hooklet can form only one bond; therefore, all the bonds can be numerated. The total interaction force between two barbs was defined as a sum of these forces:

$$F = \sum_{i=1}^N f_{\text{int}}(i), \quad (3.7)$$

where  $i$  as an index,  $N$  is the number of bonds. This is a force which has to be applied to the pulled edge of the upper barb to let it move with a constant velocity.

The motion of barb/barbule segments was calculated according to a standard equation of a particle motion in a viscous medium:

$$m\ddot{r} + \gamma\dot{r} - \sum f = 0, \quad (3.8)$$

where  $m$  is a mass of segment ( $m = 1$ ),  $\gamma$  is a coefficient damping oscillations in a system ( $\gamma = 1.1$ ),  $\sum f$  is a sum of all the forces acting on the segment. The integration time step was taken 0.02 s.

The further the upper barb moves from its initial position the greater is the number of broken bonds. Owing to the barbule's elasticity, clearly visible in figure 4a (as well as in the electronic supplementary material, movie S1), at some intervals, the system can gradually deform to some extent without breaking any bond. The longer such intervals last, the larger is the force  $F$ , and the higher the probability of simultaneous separation of many hooklets at once or generation of an avalanche of the consequent bond-breaking becomes (figure 1c–e and the electronic supplementary material, movie S1). Such collective effect makes the feather unzipping process nontrivial.

To describe the collective behaviour of the bonds quantitatively, we introduce a specific measure. The difference  $\Delta N(t) = N(t + \tau) - N(t)$  between total number of connected bonds at the beginning  $N(t)$  and at the end  $N(t + \tau)$  of a time interval  $[t, t + \tau]$ . Being normalized to the length of the interval  $\tau$ , this value coincides with a time derivative of function  $N(t)$  averaged over the corresponding time interval:

$$\left\langle \frac{dN}{dt} \right\rangle_{\tau} \equiv \frac{N(t + \tau) - N(t)}{\tau}. \quad (3.9)$$

This value is a convenient measure to characterize a rate of bond-breaking and -restoring. The time interval chosen was  $\tau = 0.5$  s. During this time, a typical avalanche of bond-breaking develops.

### 3.3. Results of numerical simulations

Typical results of numerical simulations are summarized in figure 5. Figure 5a–c presents the dependences of  $N$ , averaged derivative  $\langle dN/dt \rangle_{\tau}$  and force  $F = \sum_{n=1}^N f_{\text{int}}(n)$  on the displacement of the pulled end of the barb, respectively. The dashed line crossing all these subplots separates an initial transient process, during which no bond-breaking occurs, from the subsequent stationary regime of bond rupture. For convenience, details of the model behaviour, shown in figure 5a–c, are given in figure 5d–f in smaller time intervals. Dashed-dotted lines here

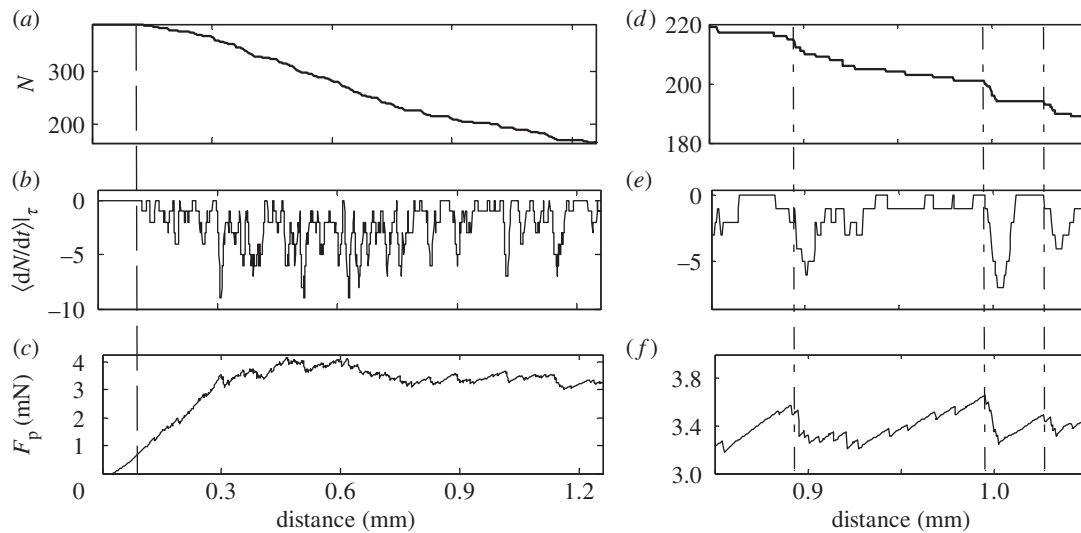


**Figure 5.** Typical evolution of the model system for the parameters specified in the text. The dependences of (a) the instant number of unbroken bonds  $N$ , (b) averaged time derivative of the number of bonds  $\langle dN/dt \rangle_\tau$  and (c) the total force  $F_p$  of interaction as functions of distance. Dashed line separates an initial transient process during which the upper subsystem moves without breaking the contacts. The same values during a small interval of developed stationary evolution are shown in detail in the right subplots (d–f). Dashed-dotted lines in these subplots mark correlations between long intervals of continued increase of the force without breaking of the bonds and subsequent avalanches of the bond-breaking (see also electronic supplementary material, movie S3).

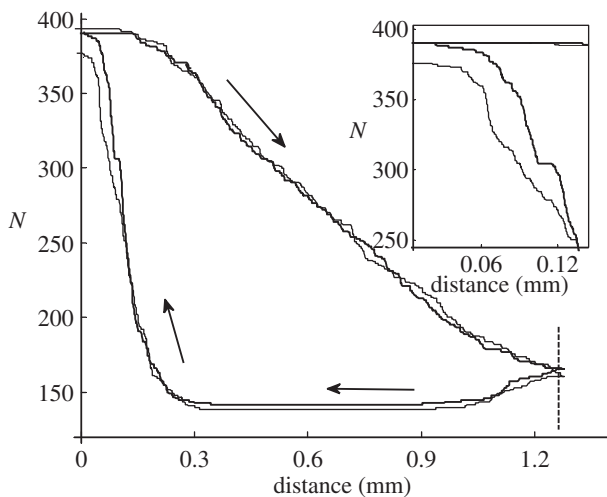


**Figure 6.** Typical unzipping–zipping cycle. The thin line represents a behaviour of the number of bonds,  $N$ , obtained during the cycle of unzipping (pulling) of the upper barb to some final displacement (shown by vertical black line) and subsequent zipping (healing) of it to the initial position. The same loop with additional lateral oscillations applied at the end of the process is shown by the bold line. In the inset, a region of small distances is magnified.

mark pronounced correlations between force drops after long periods of its continual growth and avalanches of bond-breaking, clearly recognizable by the minimums of  $\langle dN/dt \rangle_\tau$ .

The upper barb gradually returns to its equilibrium position when the external pulling force disappears. At some stage of the recovery process (healing), the broken bonds start to be restored. A bond appears again when the distance between a hooklet and its correct contact position became less than  $r_{th}$ . The thin line in figure 6 represents evolution of  $N$  during a typical unzipping–zipping cycle. First, the unzipping takes place until displacement reaches a terminal distance, indicated by the vertical black line. Then, the healing takes place until the displacement reaches the initial position. One can see that the healing ends up with a number of contacts smaller than it was

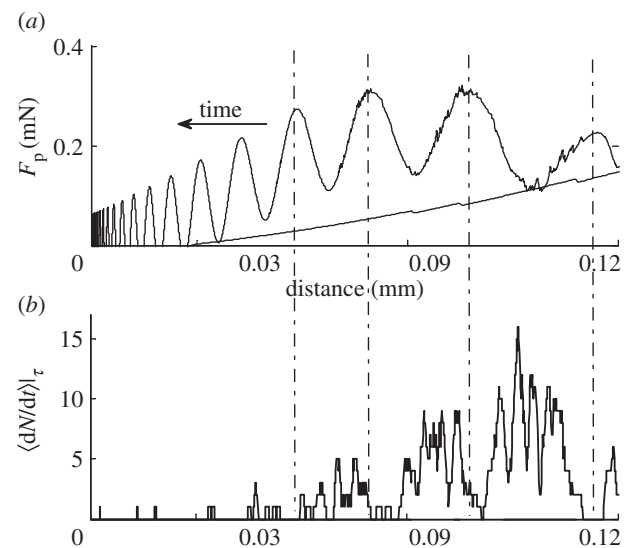


**Figure 7.** Last phase of the healing process, when lateral force oscillations are applied. The distance decreases with a time. (a) Oscillations of the pulling force induced by lateral force oscillations. (b) The avalanches of the contact recoveries represented by the positive bursts of the derivative  $\langle dN/dt \rangle_\tau$ . Dashed-dotted lines mark the positions of pulling force maximums (corresponding to a maximal shift of elastic fibres in left direction; figure 4a).

in the initial state. This is clearly seen from the inset in figure 6 (thin line). The recovery is not complete, because not all hooklets find the correct contact position to restore the bonds, even if the barbs and barbules have returned to their original configuration.

The same might happen in a real feather. However, such a stalemate can be effectively overcome by an action simulating the behaviour of a bird, which actually helps to restore the hooklet contacts by periodic motions of its beak (preening) or producing feather vibrations during flight. To simulate these in the model, we applied periodic force along the horizontal  $x$ -direction to the internal rows of the nodes, which start to oscillate. The period of the oscillations was optimized. It was adjusted to a time close to that typical for the usual

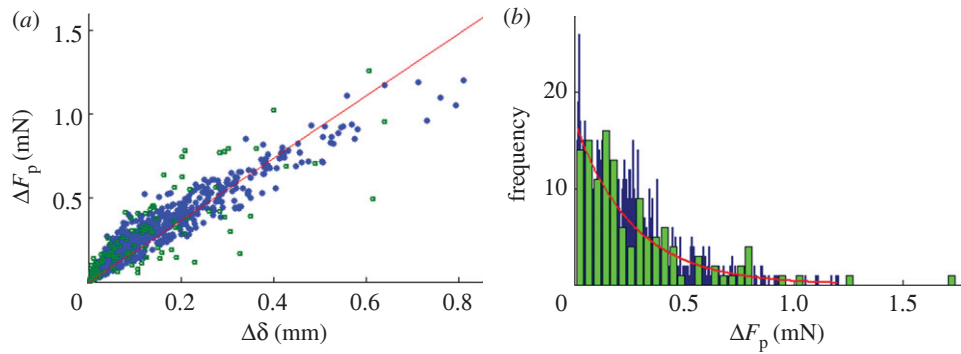


**Figure 8.** (a) Dependence of the force required for a single separation event ( $\Delta F_p$ ) on the pulling distance ( $\Delta\delta$ ) travelled by the force sensor in the model (closed blue circles) and in experiment (open green circles). Time in the model was scaled to have the same fit parameters for the regression function as in the experiment. (b) Frequency histogram of  $\delta F_p$  for the model (blue bars) and for the experiment (green bars). Force constants in the model were scaled to have the same exponent in the exponential fit as in the experiment. 931 single model separation events were analysed to prepare the graphs,  $k^{\parallel} = 3.8$ .

zipping–unzipping avalanche of the bonds. Thick line in figure 6 presents an unzipping–zipping loop of the number of contacts,  $N$ , in the presence of the periodic force applied at the end of the healing process (the barbs were close to the initial position, but many of the bonds were not yet restored). It is clearly seen from the plot that this line deviates from the thin line, starting from the moment when the periodic force was applied. After this moment, the curve in the presence of the forced oscillations goes higher than that without (thin line), and, finally, it ends with the number of contacts which practically coincides with the initial number for the original unperturbed system.

Figure 7 shows an obvious correlation between lateral oscillations of the force and rate of bond recovery. Dashed-dotted lines mark the correspondence between the force maximums (associated with the maximal displacement of the elastic fibres) and stimulated avalanches of the bond recoveries, quantitatively represented by the positive bursts of the derivative  $\langle dN/dt \rangle_{\tau}$ .

## 4. Discussion

The zigzag shape of the distance–force dependence during the separation of interlocking hooklets on hook barbules from the spine-like outgrowths on bow barbules is important for mechanical stability of covering feathers under external forces caused by air microturbulence in flight. The variation of the rupture force from 0.014 to 1.7 mN demonstrates that a feather can withstand not some average pulling force (0.27 mN), but a much higher one (1.7 mN as a maximum in our case). Such high rupture force may be observed because of the cooperative effect arising from the inhomogeneous hooklet binding strength distribution. If all the bonds are equally strong, then the constant average rupture force is measured [14]. A strong correlation between the force increment ( $\Delta F_p$ ) and the pulling distance ( $\Delta\delta$ ) required for a single separation event, figure 3a, means that the feather during the stationary phase of pulling possesses almost constant stiffness. Our model demonstrated the same correlation (figure 8a). The ratio between  $k^{\parallel}$  and  $k_{\text{int}}$  was varied in the model to achieve the correlation between  $\Delta F_p$  and  $\Delta\delta$  close to that observed in experiment. Absolute value of  $k^{\parallel}$  was also varied to achieve a shape of the force increment ( $\Delta F_p$ ) histogram in the model similar to the shape of the experimental histogram (the number of bins was also varied).

Typically, the histogram of jump (avalanche) sizes in the motion of the main plasticity carriers [11] or in Barkhausen noise of ferromagnetic materials [12] follows a power law distribution. However, in our model and in experiments with real feathers, the best fit of the histograms of the force increment distribution  $\Delta F_p$  is an exponential function (figures 3b and 8b). This indicates an independence of a separation event from the previous one. This conclusion is supported by a low correlation coefficient for the consecutive force increments ( $R^2 = -0.087$ ).

An interesting feature of such an interlocking mechanism is that microstructures are not damaged after separation, but can resist multiple zipping–unzipping cycles. The origin of hooklets permitted the origin of compacted closed and aerodynamic efficient vanes in large asymmetric contour feathers [15,16]. The hooklets are grasping devices holding together barbules and barbs, which are built from keratin with Young's modulus of about 2.5 GPa [17]. Microhooks responsible for keeping mechanical stability of the wing structure during flight are known from insects, such as representatives of Heteroptera and Hymenoptera. Here, hooks provide functional diptery. Forewing microhook arrays holding the hindwings of the bug *Coreus marginatus* in flight can be separated from the hindwing at a force of 0.8 mN. The array consists of numerous (more than 20) 40–60  $\mu\text{m}$  long hooks [18]. The number of wing hooks holding fore- and hindwings together correlates with the flight distance for bees [19].

Because in the plumage of birds the feathers have different morphology, it would be interesting to compare how the rupture force differs in different types of feathers and how the force is related to the stiffness of the vane, and to a particular function of the feather. Interspecific comparison might provide some insights into the microstructural adaptations to feather specializations.

The numerical model presented here differs from similar models of artificial systems such as Velcro models in geometry [20] and in the introduction of bonding strength distribution compared with [14]. Our model demonstrates the features of real feathers observed in mechanical experiments. It demonstrated the same shape of the force–distance curves and system healing when an external force disappeared. Moreover, the model demonstrated a more effective system healing when a periodic force, modelled birds preening, was applied to the feather vane.

**Acknowledgements.** Victoria Kastner (Max Planck Institute for Intelligent Systems, Stuttgart, Germany) helped with the linguistic corrections of the manuscript.

**Funding statement.** This work was supported by the German Science Foundation (DFG) Initiative 'Bionik' (DFG grant no. GO995/7-1 to SG).

## References

1. Clarke J. 2013 Feathers before flight. *Science* **340**, 690–692. (doi:10.1126/science.1235463)
2. Alibardi L, Knapp LW, Sawyer RH. 2006 Beta-keratin localization in developing alligator scales and feathers in relation to the development and evolution of feathers. *J. Submicrosc. Cytol. Pathol.* **38**, 175–192.
3. Xu X, Wang K, Zhang K, Ma Q, Xing L, Sullivan C, Hu D, Cheng S, Wang S. 2012 A gigantic feathered dinosaur from the Lower Cretaceous of China. *Nature* **484**, 92–95. (doi:10.1038/nature10906)
4. Saino N, Stradi R, Ninni P, Pini E, Moller AP. 1999 Carotenoid plasma concentration, immune profile, and plumage ornamentation of male barn swallows (*Hirundo rustica*). *Am. Nat.* **154**, 441–448. (doi:10.1086/303246)
5. Sumida S, Brochu CA. 2000 Phylogenetic context for the origin of feathers. *Am. Zool.* **40**, 486–503. (doi:10.1668/0003-1569(2000)040[0486:PCFT00]2.0.CO;2)
6. Chen PJ, Dong ZM, Zhen SN. 1998 An exceptionally well-preserved theropod dinosaur from the Yixian formation of China. *Nature* **391**, 147–152. (doi:10.1038/34356)
7. Pettingill Jr OS. 1970 *Ornithology in laboratory and field*, 4th edn. Minneapolis, MN: Burgess.
8. Carboneras C. 1992 Family Anatidae (ducks, geese and swans). In *Handbook of the birds of the world*, vol. 1 (eds J del Hoyo, A Elliott, J Sargatal), pp. 536–630. Barcelona, Spain: Lynx Edicions.
9. Dimond CC, Cabin RJ, Brooks JS. 2011 Feathers, dinosaurs, and behavioral cues: defining the visual display hypothesis for the adaptive function of feathers in non-avian theropods. *BIOS* **82**, 58–63. (doi:10.1893/011.082.0302)
10. Miller SA, Harley JP. 1996 *Zoology*. Dubuque, IA: Wm. C. Brown Publishers.
11. Lebyodkin MA, Dunin-Barkovskij LR, Lebedkina TA. 2002 Universality and scaling of unstable plastic flow. *JETP Lett.* **76**, 612–615. [Translated from *Pis'ma v Zhurnal Éksperimental'noj i Teoreticheskoy Fiziki* **76**, 714–718.] (doi:10.1134/1.1541046)
12. Durin G, Zapperi S. 2000 Scaling exponents for Barkhausen avalanches in polycrystalline and amorphous ferromagnets. *Phys. Rev. Lett.* **84**, 4705–4708. (doi:10.1103/PhysRevLett.84.4705)
13. Gorb SN, Popov VL. 2002 Probabilistic fasteners with parabolic elements: biological system, artificial model and theoretical consideration. *Phil. Trans. R. Soc. Lond. A* **360**, 211–225. (doi:10.1098/rsta.2001.0926)
14. Maddalena F, Percivale D, Puglisi G, Truskinovsky L. 2009 Mechanics of reversible unzipping. *Continuum Mech. Thermodyn.* **21**, 251–268. (doi:10.1007/s00161-009-0108-2)
15. Alibardi L. 2005 Fine structure of juvenile feathers of the zebra finch in relation to the evolution and diversification of pennaceous feathers. *J. Submicrosc. Cytol. Pathol.* **37**, 323–343.
16. Alibardi L. 2007 Cell organisation of barb ridges in regenerating feathers of the quail: implications of the elongation of barb ridges for the evolution and diversification of feathers. *Acta Zool.* **88**, 101–117. (doi:10.1111/j.1463-6395.2007.00257.x)
17. Bonser RHC, Purslow PP. 1995 The Young's modulus of feather keratin. *J. Exp. Biol.* **198**, 1029–1033.
18. Perez-Goodwyn PJ, Gorb SN. 2004 Frictional properties of contacting surfaces in the hemelytra-hindwing locking mechanism in the bug *Coreus marginatus* (Heteroptera, Coreidae). *J. Comp. Physiol. A* **190**, 575–580. (doi:10.1007/s00359-004-0520-9)
19. Abrol DP. 1986 Flight range and significance of wing hooks in *Megachile femorata* Smith (Hymenoptera, Megachilidae). *J. Anim. Morphol. Physiol.* **3**, 107–112.
20. Pugno NM. 2007 Velcro nonlinear mechanics. *Appl. Phys. Lett.* **90**, 121918. (doi:10.1063/1.2715478)